


Theoretical Calculations and Experimental Measurements on the Two-Component Au-Pt Alloys with Ultralow Magnetic Susceptibility

Ao Lou,^{1,§} Yuanyang Yu,^{1,§} Butian Zhang,² Yi Liu,³ Quan Fu,³ Jiankang Zhang,³ Hua-Hua Fu^{⊗,1,*},
Shun Wang^{⊗,1,2,†} and Ze-Bing Zhou^{1,2,‡}

¹*School of Physics, Huazhong University of Science and Technology, Wuhan 430074, China*

²*MOE Key Laboratory of Fundamental Physical Quantities Measurement and Hubei Key Laboratory of Gravitation and Quantum Physics, PGMF, Huazhong University of Science and Technology, Wuhan 430074, China*

³*State Key Laboratory of Advanced Technologies for Comprehensive Utilization of Platinum Metal, Kunming Institute of Precious Metals, Sino-Platinum Metals Co. Ltd., Kunming 650106, China*

 (Received 31 May 2022; revised 15 February 2023; accepted 16 February 2023; published 24 March 2023)

A solid-state material with ultralow magnetic susceptibility χ is the key material candidate in aeronautical devices and special targeted drugs. In this work, we design a series of two-component alloy samples $\text{Au}_{1-x}\text{Pt}_x$, and study their magnetic structures and susceptibilities by using the first-principles calculations within a spin-polarized relativistic Korringa-Kohn-Rostoker coherent potential approximation. Our theoretical results demonstrate that by controlling the ratio parameter x , ultralow magnetic susceptibilities ($\chi < 10^{-6}$ cm³/mol) occur in AuPt alloys around the sample $\text{Au}_{0.75}\text{Pt}_{0.25}$. Following the theoretical calculations, several realistic AuPt alloy samples with ultralow magnetic susceptibilities are fabricated successfully in experiments, and the experimental measurements on magnetic susceptibilities are well consistent with our theoretical predications. This work not only provides us changes to study physical properties of the materials with ultralow magnetic susceptibility, but also constructs unique materials towards special device applications in TianQin project and others.

DOI: [10.1103/PhysRevApplied.19.034080](https://doi.org/10.1103/PhysRevApplied.19.034080)

I. INTRODUCTION

When mixing a paramagnetic metal with a diamagnetic one with a proper ratio, a unique material exhibiting ultralow magnetic susceptibility (i.e., χ on the order of 10^{-6} in unit of cm³/mol) may be constructed to meet special device applications. AuPt alloys, famous ones belonging to this kind of material, have a wide range of applications due to unique magnetic properties together with their chemical stability. For instance, in space-based gravitational-wave-detection experiments such as LISA [1,2] and TianQin [3–5], free-falling test masses are required to travel along geodesics, undisturbed by other forces. To suppress the disturbance from temperature, cosmic rays and space plasma, the test masses must have high electrical conductivity, high thermal conductivity, good chemical stability, and most usefully, low magnetic susceptibility ($\chi < 10^{-6}$ cm³/mol) [6–8]. To date, AuPt

alloys have been considered as the potential material candidates for test masses, and many researches have been devoted to their preparations and the measurements on magnetic properties [9,10]. Another application is in the area of biomedical engineering. When magnetic resonance imaging (MRI) is performed on patients with metal containing implantable medical devices such as intravascular stents, emboli coils, and intracranial electrodes, imaging artifacts may appear, raising difficulties in diagnostics [11]. The main reason for artifacts is the mismatch between the magnetic susceptibility of the metals and human tissue. Therefore, the development of metals with magnetic susceptibility close to human tissue ($\chi \sim -9 \times 10^{-6}$ cm³/mol) is the key to solve this problem [12]. Fortunately, AuPt alloys can be worked as promising candidates for their tunable ultralow magnetic susceptibility and biocompatibility [13,14].

Despite the fact that the study of $\text{Au}_{1-x}\text{Pt}_x$ alloys has made significant progress in the past 10 years, it still faces challenges. Firstly, the experimental results suggest that there are many factors affecting the magnetic properties of AuPt alloys, such as the chemical composition, the preparation process, annealing temperature, and impurity

*hhfu@hust.edu.cn

†shun@hust.edu.cn

‡zhouzb@hust.edu.cn

§A.L. and Y.Y. contributed equally to this work.

content, etc. [15,16]. Secondly, in some previous works, the magnetic susceptibility in AuPt alloy samples have been predicted in theory, however, the proposed values of ultralow magnetic susceptibility have not been confirmed in realistic alloy samples. Thirdly, there is still no clear understanding into the physical mechanism and origination of the weak magnetism of AuPt alloys with χ on the order of 10^{-6} cm³/mol, especially the contributions from different spins, orbits, and their couplings. Considering the developed applications of particular materials with ultralow magnetic susceptibility in LISA, TianQin projects and in medical devices as mentioned previously, the experimental fabrications on AuPt alloys possessing ultralow χ values are required and have already been one of the hot topics in the field of metal alloys, which drives us to construct the AuPt alloy samples with the special magnetic properties based on theoretical calculations and experimental fabrications.

In this work, we first design Au_{1-x}Pt_x alloy samples by using virtual crystal approximation (VCA) [17–20], and explore the magnetic structure of AuPt alloys in details, including the contributions from the spins, orbits, and their couplings in Au and Pt atoms. Then, we calculate the magnetic susceptibility of AuPt alloy samples by performing the first-principles calculations within a spin-polarized relativistic Korringa-Kohn-Rostoker coherent potential approximation (KKR CPA) [21–25]. Within the above theoretical framework, the magnetic susceptibility of AuPt alloy samples can be calculated low to 10^{-6} cm³/mol, indicating that a series of AuPt alloys with ultralow magnetic susceptibilities have been obtained in theory. Following the theoretical calculations, we synthesize successfully several realistic Au_{1-x}Pt_x alloys with ultralow magnetic susceptibilities in experiments, in which the component ratios and the magnetic susceptibilities are in good agreements with our theoretical predictions. Our work provides a feasible realistic alloy hosting the ultralow magnetic susceptibility that meets the particular requirements in TianQin project and other special device applications.

The remainder of this paper is organized as follows. In Sec. II, we construct the AuPt alloy samples by using the VCA approach, then introduce the theoretical methods to calculate the magnetic properties of AuPt alloys. In Sec. III, we analyze in details the magnetic structure and origination of magnetic susceptibilities in AuPt alloys, and uncover the relations of the magnetic susceptibilities of Au_{1-x}Pt_x alloys versus the component ratio between Au and Pt. In Sec. IV, some realistic AuPt alloy samples with ultralow magnetic susceptibility are prepared successfully in experiments, and the comparisons on magnetic susceptibilities between theoretical calculations and experimental measurements are performed. Finally, some conclusions are summarized in the last section.

II. ALLOY STRUCTURES AND THEORETICAL METHODS

To construct Au_{1-x}Pt_x alloy samples, we usually adopt suitable numbers of Au and Pt atoms to design an alloy supercell, in which the component ratio between Au and Pt agrees with the given value x , then optimize the alloy structures by using the first-principles calculations within a density-functional theory (DFT) framework [26,27]. However, to design an alloy sample possessing ultralow magnetic susceptibility, the atomic number of one component may be much less than that of the other one in a supercell, resulting in a remarkably large unit cell established to calculate magnetic susceptibility and other properties with high accuracies. On the other hand, the uniform distribution of minority also requires us to design the alloy supercell as large as possible. The above two requirements make the AuPt alloys much more complex, enhancing largely the difficulty to perform the first-principles calculations. Thus, if we construct AuPt alloys directly by a conventional way, the numerical accuracy on ultralow magnetic susceptibility may be much more difficult to ensure.

To deal with the above hard task, in this work, we construct the Au_{1-x}Pt_x alloys by using the VCA approach [17–20]. In this approach, the simplified configuration of alloys restores the Bloch symmetry by replacing the components of a binary disordered alloy $A_{x_A}B_{x_B}$ by a hypothetical element having the average atomic number $\bar{Z} = x_A Z_A + x_B Z_B$, which indicates that to simulate an alloy, we may distribute the different atoms evenly in every atom according to the ratio parameter x . By adopting the above relation on the ratio x , here we mix the Au and Pt atom to construct a virtual atom with another atomic number. Then the alloy constructed these virtual atoms can be characterized by Au_{1-x}Pt_x with the ratio values of x ($= 0.0 \sim 1.0$), as illustrated in Fig. 1. Note that to treat the disorder in alloys, we adopt the coherent potential approximation for all virtual atoms, implying that to search for an ordered lattice of effective scatters, the motion of an electron in effective lattices of virtual atoms would approximate the configurationally averaged motion of an electron in the random lattice [31–34].

Then the structures of all alloy samples are optimized by using the first-principles calculations based on the Vosko-Wilk-Nusair (VWN) exchange-corrections potentials, which is the most common parametrization within the local density-functional approximation [26,27]. The optimized lattice constants of AuPt alloys versus the ratio parameter x are achieved as drawn in Fig. 1. To make sure the validity of our optimized calculations, the experimental values of lattice constants in three alloy examples, i.e., the pure Au single crystal (Exp-I [28]), the alloy Au_{0.5}Pt_{0.5} (Exp-II [29]) and the pure Pt single crystal (Exp-III [30]), are also provided for comparison. One may find that the lattice constants of Au_{1-x}Pt_x alloys nearly increase linearly

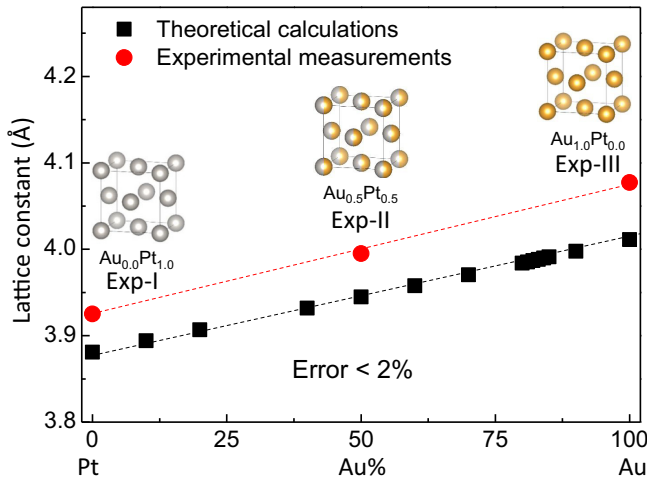


FIG. 1. The virtual crystal approximation approach within the density-functional theory framework to construct the $\text{Au}_{1-x}\text{Pt}_x$ alloy systems. The proportional parameter x is adopted from 0 to 1.0, and the lattice constants of three realistic materials Pt, $\text{Pt}_{0.5}\text{Au}_{0.5}$, and Au is obtained from theoretical works, i.e., Exp-I in Ref. [28], Exp-II in Ref. [29], and Exp-III in Ref. [30]. The error between the data from theoretical calculations and experimental measurements is less than 2%.

with the increasing of x , which are well consistent with the relation gained from experimental measurements. Moreover, the data errors between the experimental results and our theoretical calculations are less than 2%, indicating the reliability of the AuPt alloy samples constructed here by using the VCA approach together with the first-principles calculations.

To study the magnetic properties of $\text{Au}_{1-x}\text{Pt}_x$ alloy samples, we use a spin-polarized relativistic SPR KKR code for calculating solid-state properties, and the related program package SPR KKR is contributed by Ebert *et al.* [21]. This package allows calculation of the electronic structure of arbitrary three-dimensional periodic systems, including in particular systems with chemical disorder. The electronic structure calculation can be done in a nonrelativistic, scalar-relativistic as well as fully relativistic mode. In the latter mode, paramagnetic as well as spin-polarized systems with an arbitrary spin configuration can be dealt with. To obtain the magnetic susceptibility of alloy samples, we apply the SPR KKR package with fully relativistic mode, as a linear response to a static uniform external magnetic field, and by fully considering the spin and orbit susceptibility, and the contributions from spin-orbit couplings in all atoms. Additionally, we apply this way to analyze further the independent contributions on the total magnetic susceptibility from all the shells, such as s , p , d , and f orbitals in Au and Pt atoms. To get more details on the theoretical methods, one may refer to some previous literatures [35–39].

III. MAGNETIC STRUCTURES AND CALCULATED RESULTS OF MAGNETIC SUSCEPTIBILITY

Before giving the numerical results of magnetic susceptibilities of AuPt alloys, we should understand the magnetic structures of alloy samples, especially the possible origination of ultralow magnetic susceptibilities in them. We well know that the single crystals Au and Pt exhibit paramagnetism and diamagnetism, respectively. Considering that both Au and Pt belong to heavy metals, the spin, orbital, and the spin-orbital coupling (SOC) in them play significant roles on the total magnetic susceptibility. In particular, the SOC may lead to the coupling of spin- and orbital-induced magnetic moments, producing an additional magnetic susceptibility in alloys [16,40–42]. By fully considering these factors, the magnetic structures of AuPt alloys can be described in Fig. 2. One can see that the total magnetic susceptibility is originated from both metal components and for every component, the magnetic susceptibility is contributed both by their spin and orbital degrees of freedom, which play different roles on magnetic moments of alloys. To consider these two key freedoms, the total spin susceptibility χ_s and the total orbital susceptibility χ_o can be expressed by the following relations [16,40]:

$$\begin{aligned}\chi_s &= \chi_{\text{spin}} + \chi_{so}, \\ \chi_o &= \chi_{\text{orb}} + \chi_{os}.\end{aligned}\quad (1)$$

where χ_{spin} and χ_{orb} refer to the spin susceptibility and orbital susceptibility in Au and Pt. Considering the SOC, these two total magnetic susceptibilities include the contributions from other two terms, i.e., χ_{so} determined by the spin-orbital coupling and χ_{os} by the orbital-spin coupling. Usually, the SOC helps to enhance spin susceptibility and is contributed mainly by s , p , d , and f orbitals. Thus the magnetic susceptibilities contributed by these four suborbitals should be calculated to understand the physical origination of magnetic susceptibility in AuPt alloys.

As for the orbital degree of freedom in Au and Pt, the related magnetic susceptibilities are composed by two parts, i.e., the total Langevin orbital susceptibility and the total Van Vleck orbital susceptibility, as described in the right panel of Fig. 2. The former is usually negative ($\chi_{\text{dia}}^o < 0$) and gives rise to diamagnetism in alloys, while the latter is usually positive ($\chi_{\text{para}}^o > 0$) and results in paramagnetism in alloys. Moreover, the total Van Vleck orbital magnetic susceptibility is also influenced remarkably both by the SOC and the orbital-orbital coupling (OOC). The former leads to the SOC-induced orbital susceptibility, and the latter leads to the so-called orbital susceptibility. As for the enhanced spin and orbital susceptibility, the four suborbitals labeled as s , p , d and f may play considerable while

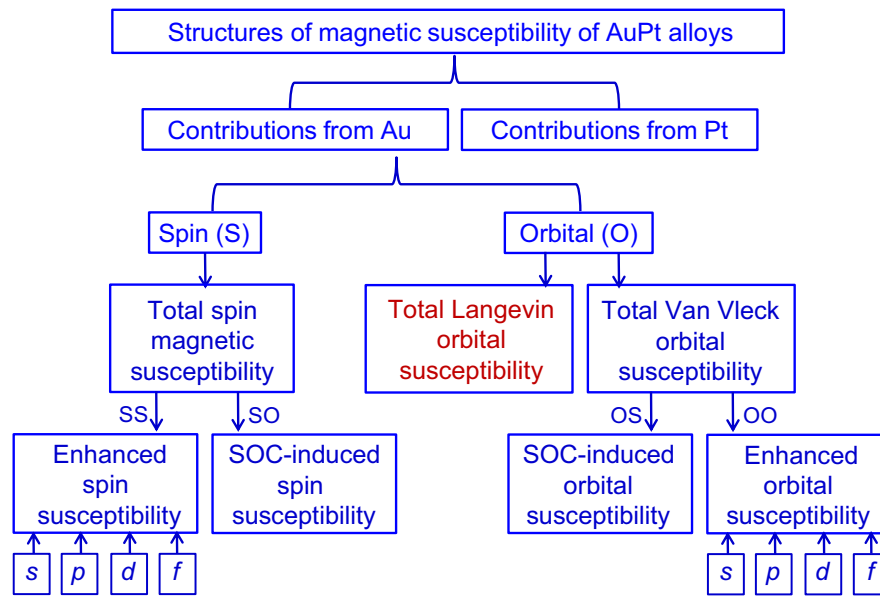


FIG. 2. Structure of the magnetic susceptibility of $\text{Au}_{1-x}\text{Pt}_x$ alloy sample. From the first-principles calculations based on the DFT within the KKR CPA, the magnetic susceptibility of alloy samples is originated from Au and Pt elements, and further contributed by their total spin and orbital magnetic susceptibility. The later includes total Langevin orbital and total Van Vleck orbital susceptibilities. These special magnetic susceptibilities are determined further by the related spin-spin (SS) and spin-orbital (SO) couplings as described in the figure, where s, p, d, f indicate four suborbitals in Au and Pt atoms.

different influences. Furthermore, it should be stressed that the competitions among the total Langevin orbital susceptibility, the total Van Vleck orbital susceptibility and the total spin magnetic susceptibility will determine the total magnetic state of alloy samples. These magnetic structures give us the theoretical foundations to calculate and understand the ultralow magnetic susceptibilities of AuPt alloys.

In what follows, we present our numerical results on the total magnetic susceptibilities χ of AuPt alloys and explore their physical origination through adjusting the ratio parameter x . First, we plot the component-dependent total magnetic susceptibilities χ_{Pt} and χ_{Au} versus x in Fig. 3(a). One may find that $\chi_{\text{Pt}} > 0$ while $\chi_{\text{Au}} < 0$, confirming that in the alloy samples, Pt displays the paramagnetic feature while Au maintains its diamagnetic one. However, these two kinds of magnetic susceptibilities are influenced remarkably by changing x . As x increases, χ_{Pt} increases largely while χ_{Au} decreases slightly to zero. Interestingly, their changing trends versus x do not show a linear behavior, indicating that the hybridizations among Au and Pt atoms show an obvious influence on the total magnetic properties of alloys. Particularly, the curve of χ_{Pt} versus x displays a round peak around $x = 0.3$, leading to the fact that χ_{tot} of alloys changes from negative to positive values, which gives us a chance to achieve the ultralow magnetic susceptibility ($\chi \sim 0$ or $< 10^{-6} \text{ cm}^3/\text{mol}$) in alloys through controlling the component ratio of Au and Pt.

To understand further the magnetic structure of total magnetic susceptibility of AuPt alloys, we turn to analyze the spin susceptibility χ_{spin} and the orbital susceptibility χ_{orb} in Au and Pt. Figure 3(b) illustrates χ_{spin} and χ_{orb} versus the ratio parameter x in Au. One can see that χ_{orb} nearly keeps a finite positive value of $1.3 \times 10^{-5} \text{ cm}^3/\text{mol}$, while χ_{spin} increases from zero to finite while positive values, indicating that χ_{spin} in Au atoms is enhanced by the hybridizations with the neighboring Pt atoms. Moreover, the diamagnetic susceptibility χ_{dia} , contributed by total Langevin orbital in Au, keeps as a negative constant of approximately $-4.0 \times 10^{-5} \text{ cm}^3/\text{mol}$, influenced little by the changing ratio x . However, the absolute values of χ_{dia} are much larger than the sum of χ_{spin} and χ_{orb} , leading to the negative χ_{Au} , which uncovers the physical origination of diamagnetism in Au. Similarly, χ_{spin} , χ_{orb} , and χ_{dia} in Pt are also calculated and illustrated in Fig. 3(c). It is obvious that for the all ratio values of x , both χ_{spin} and χ_{orb} are positive and larger than $4.0 \times 10^{-5} \text{ cm}^3/\text{mol}$, while χ_{dia} still keeps as the negative value of $-4.0 \times 10^{-5} \text{ cm}^3/\text{mol}$, leading to the positive χ_{Pt} , i.e., the paramagnetism of Pt in all AuPt alloys.

As discussed previously, owing to the fact that both Au and Pt belong to heavy metals, the SOC in them play a key role on their respective magnetic susceptibility, thus it can be considered as another useful factor to influence the total magnetic susceptibility in AuPt alloys. To explain this conclusion, we calculate the SOC-induced χ_{spin} and χ_{orb} in Au and Pt versus x as illustrated in Fig. 3(d). We

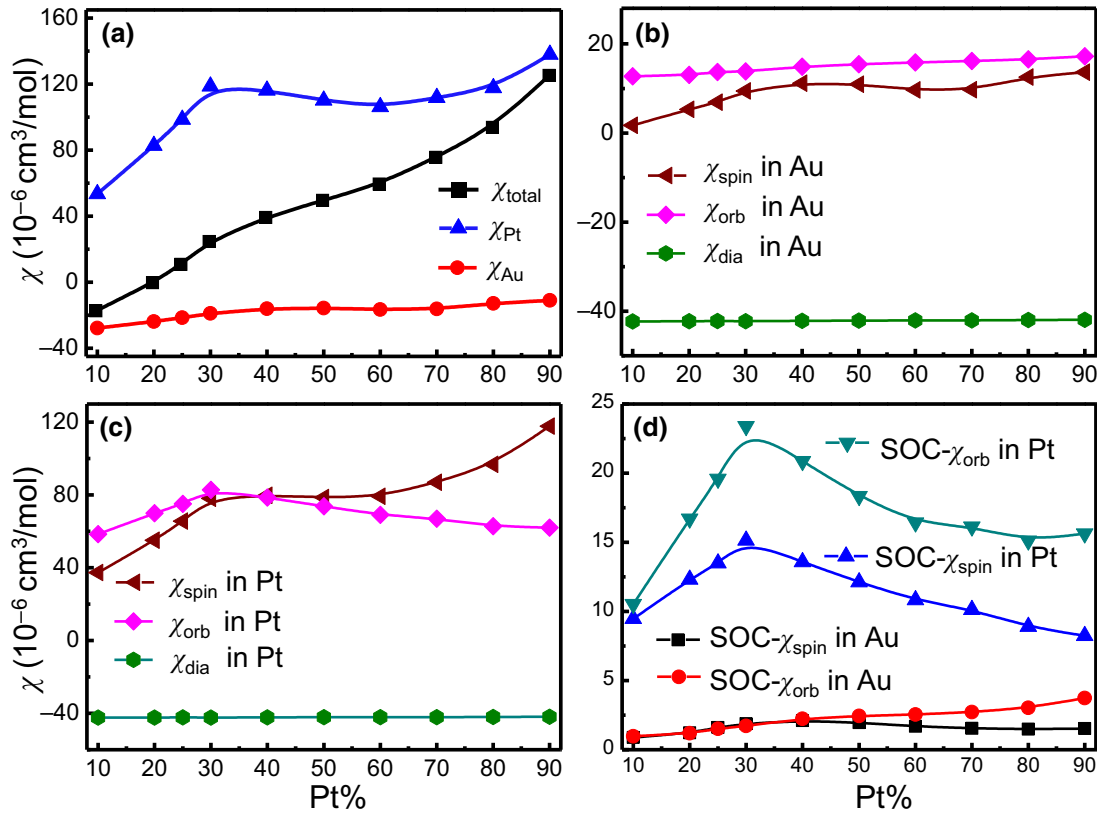


FIG. 3. (a) The dependent magnetic susceptibilities contributed by Pt and Au element in the alloy examples $Au_{1-x}Pt_x$. (b) The renormalized magnetic susceptibilities contributed by Au and Pt, and the total magnetic susceptibility of alloy examples versus the content ratio of Pt. (c),(d) The total spin susceptibility, the total orbital susceptibility, and the diamagnetic susceptibility in Au and Pt, respectively.

find that the SOC-induced χ_{spin} and χ_{orb} in Pt and Au are both positive, which are contributable to the formation of paramagnetism in AuPt alloys. Moreover, one can see that for $x = 10\%$, the SOC-induced χ_{spin} and χ_{orb} are nearly equal to zero in Au, indicating that χ_{spin} and χ_{orb} in the total magnetic susceptibility in AuPt alloys are dominated by Au atoms. Apart from these, the SOC-induced χ_{spin} and χ_{orb} are much larger than the corresponding values in Au. Particularly, as the parameter x increases, the SOC-induced χ_{spin} and χ_{orb} in Pt increases firstly to their largest values and then decreases, indicating that the round-peak structure in the curve of total magnetic susceptibility χ_{Pt} is mainly contributed by the SOC-induced magnetic susceptibilities. Therefore, we believe that the electrons' hybridizations between Au and Pt influence largely the formation of magnetic states in AuPt alloys.

To uncover further the physical nature of χ_{spin} and χ_{orb} in Au and Pt, we turn to analyze the contributions from four dominate orbitals, i.e., s , p , d , f orbitals in them, on some typical kinds of magnetic susceptibilities in alloys. In Fig. 4(a), we plot the contributions from these four orbitals on χ_{spin} in Au. From first glance, one can find that the above four orbitals play different roles on χ_{spin} .

As the ratio parameter x increases, the magnetic susceptibility contributed by the d orbital increases nearly linearly, and its values are much larger than those from the other three orbitals, indicating that χ_{spin} in Au is dominated by d orbital. However, the magnetic susceptibility from s orbital is much more complex, because its values change from negative to positive, making its curves versus x to display as two round-peak structures. This is because the electrons in the s orbital belong to the outer-layer ones and may be influenced more easily by the hybridizations from other kind of atoms. The magnetic susceptibility from the p orbital displays an opposite changing trend and are influenced much more weakly than these in the above s and d orbitals. Additionally, the magnetic susceptibility from the f orbital remains zero nearly in the all alloy samples, indicating that the f orbital shows little influence on χ_{spin} in Au.

By a similar way, the contributions from the s , p , d , f orbitals on χ_{orb} in Au are also presented as illustrated in Fig. 4(b). We find that the χ_{orb} values from the above four orbitals remain positive and increase nearly linearly while slightly as the ratio parameter x increases. Moreover, χ_{orb} from the d orbital is much larger than the corresponding

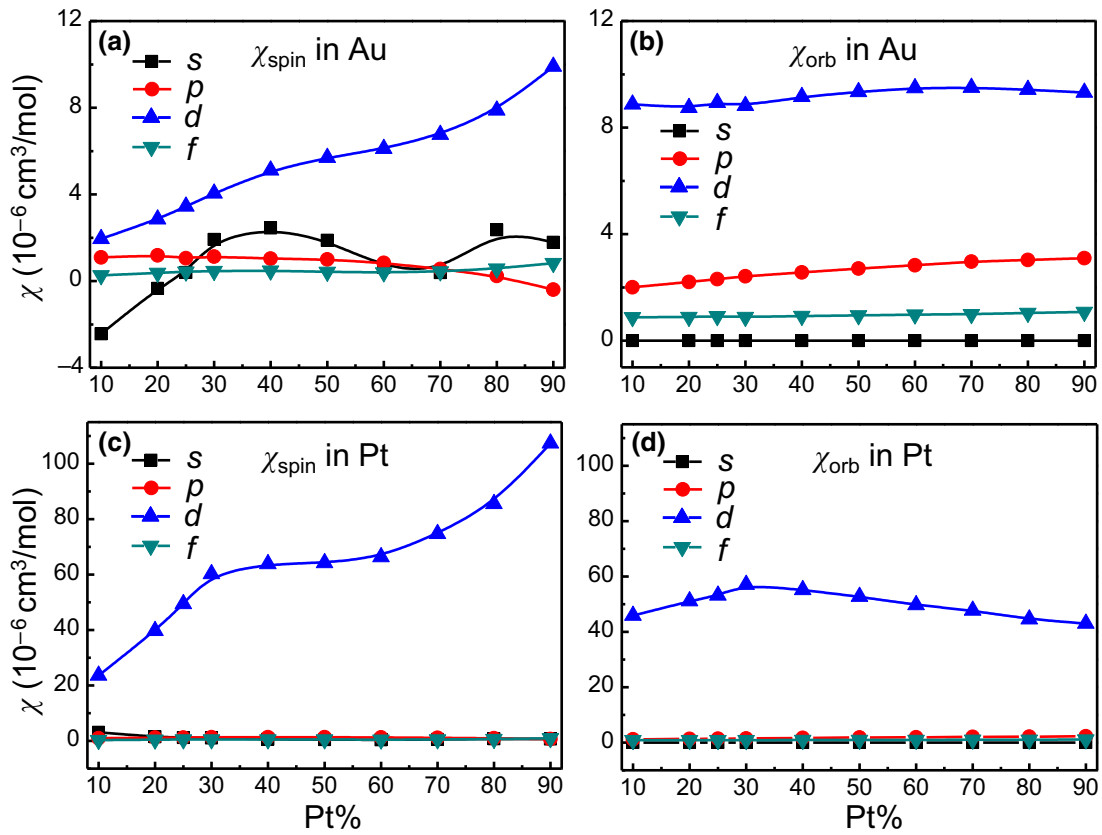


FIG. 4. Contributions from the s , p , d , and f orbital on the spin susceptibility (a) and the orbital susceptibility (b) in Au, and the related contributions from the above four orbitals on the spin susceptibility (c) and the orbital susceptibility (d) in Pt in the $\text{Au}_{1-x}\text{Pt}_x$ alloy examples.

values from the other three orbitals, indicating that χ_{orb} in Au is dominated also by its d orbital. Nevertheless, the contribution on χ_{orb} from the s orbital remains zero in the all AuPt alloy samples, which is due to the fact the the s orbital is localized uniformly and symmetrically in the outermost layer in Au.

To present a comparable study, the contributions from the above four orbitals on χ_{spin} and χ_{orb} in Pt are also calculated and illustrated in Figs. 4(c) and 4(d), respectively. It is clearly shown that both χ_{spin} and χ_{orb} in Pt are contributed only by the d orbital, since the susceptibilities from the other three orbitals remain nearly zero in all AuPt alloys, which gives the physical nature of the paramagnetism in AuPt alloys. Moreover, with the increasing of x , the contribution from the d orbital on χ_{spin} is enhanced remarkably. This changing trend versus x is much more similar to that of total spin susceptibility in the same orbital in Au. Nevertheless, χ_{orb} increases firstly then decreases as x increases, which is similar to the changing trend of χ_{orb} in the same orbital in Au. Moreover, χ_{spin} and χ_{orb} from the d orbital in Pt are much larger than the corresponding susceptibility values from the d orbital in Au, which can be considered as the main reason leading to the difference between the paramagnetic state in Pt and the diamagnetic

state in Au. Therefore, the main magnetic structures in the AuPt alloys can be summarized below: (i) χ_{spin} and χ_{orb} in Au and Pt influence largely the total magnetic susceptibilities in alloys, while these two susceptibilities in Au are much smaller than the related values in Pt, leading to diamagnetism in Au and paramagnetism in Pt; (ii) χ_{spin} and χ_{orb} in both Au and Pt are contributed mainly by the d orbital in both metals and (iii), the changing trends in some kinds of magnetic susceptibilities versus the ratio parameter x in Au and Pt display nonlinear behaviors, indicating the hybridizations between Au and Pt atoms play a key role on the magnetic properties of AuPt alloys.

IV. EXPERIMENTAL FABRICATIONS OF AuPt ALLOYS AND COMPARISONS WITH THEORETICAL RESULTS

Following the above theoretical calculations on magnetic susceptibilities, in this section, we turn to synthesize some real AuPt alloy samples with ultralow magnetic susceptibility. In our experiments, the AuPt alloy ingots are prepared from high-purity gold (99.99%) and platinum (99.98%) by medium-frequency induction melting under vacuum condition. The ingots are homogenized at 1000 °C

for 10 h and hot rolled to 20 mm with finishing temperature of 850 °C. Afterwards, hot-rolled plates are cold rolled with 50% reduction and annealed at 950 °C for 5 h under ambient air, followed by rapid cooling with water. The combination process of cold rolling and thermal treatment are repeated for 3 times to prepare a homogeneous alloy. The alloy plates are finally cut into a cylindrical form (diameter of 3 mm and length of 4 mm), and then soaked ultrasonically in hot HCl solution (40%) for 5 min to remove potential contamination on the surface for ensuring measurement accuracy of volume magnetic susceptibility. To examine the sample qualities of AuPt alloys we synthesize, we perform XRD measurements on pure Au, pure Pt, and AuPt alloys, and the related data are provided in Fig. S1 within the Supplemental Material [43]. Moreover, we also perform the glow-discharge mass spectrometry (GDMS) and the inductive coupled-plasma (ICP) measurements, and their data are provided in Tables S1 and S2 with the Supplemental Material, respectively [43]. These additional experimental measurements ensure fully the high sample qualities of our AuPt alloys.

Before magnetic measurements, we soak the AuPt samples with hydrochloric acid to remove magnetic impurities (Fe, Co and Ni and etc.) on the surface of alloy samples. In the experiment, we find that heating AuPt alloys in hydrochloric acid (HCl) to 100 °C has the best effect on removing the magnetic impurities contained in samples. The experimental procedures are described as follows: first, the samples are soaked in 5% HCl for 10 min, then they are cleaned by the deionized water. At last, they are baked in an oven at 100 °C for 5 min to remove

the moisture on the surface of the samples. After this, the samples are tested by using VSM measurement. Note that before using VSM for magnetic measurement, the background noise of the instrument should be deducted, because the measured sample has a remarkably small susceptibility, which is easy to be affected by the instrument's background noise. It is stressed that the alloys with nominal composition of $\text{Au}_{1-x}\text{Pt}_x$ ($x = 1.0, 0.30, 0.28, 0.25, 0.24, 0.20,$ and 0.0 in %) are prepared using Au and Pt with purity better than 99.9% as starting materials as shown in Fig. 5(b). The AuPt alloys are chosen to prepare the small-size ingot with a diameter of 3 mm and a height of 3–6 mm. The content of impurities is strictly controlled during the preparation of the alloys, where the content of ferromagnetic elements does not exceed 1 ppm. Note that a real AuPt alloy sample is drawn in the inset of Fig. 5(b), and the related size parameters are also provided.

To present quantitative comparisons between the experimental measurements and our theoretical calculations, we should make clear the influence of SOCs in Au and Pt components on the magnetic susceptibilities of alloy samples. It is noted that within the framework of the SPR CPA approach, the SOC strength of every component can be manipulated by a scaling factor C_i , where i indicates the component number in alloy. Here $C_{1(2)}$ denotes the scaling factor of SOC in Au (Pt) and as $C_i = 0$, the SOCs in systems are suppressed to zero (i.e., the nonrelativistic case); while as $C_i = 1$, the material samples correspond to real alloy systems [41,42]. In Fig. 5(a), we plot the magnetic susceptibilities of $\text{Au}_{1-x}\text{Pt}_x$ alloy samples with $0 \leq x \leq 1.0$ as the scaling factors $C_{1(2)}$ are changed from 0.65

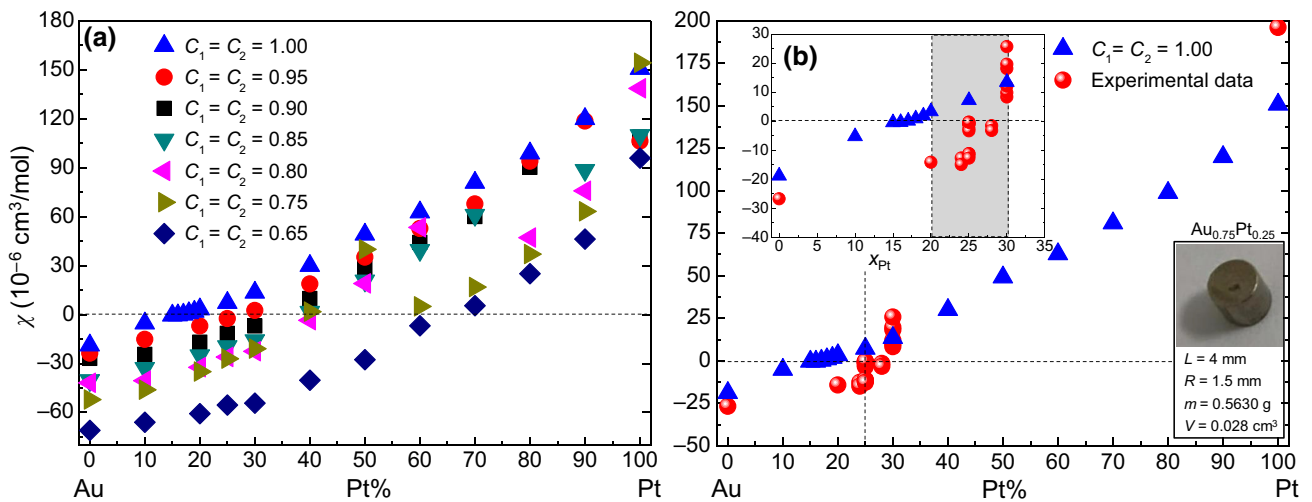


FIG. 5. (a) Calculated results of magnetic susceptibilities χ of $\text{Au}_{1-x}\text{Pt}_x$ versus the component ratio x for different scaling parameters $C_{1(2)}$ of SOCs. (b) The magnetic susceptibilities χ of 14 alloy samples of $\text{Au}_{1-x}\text{Pt}_x$ with $x = 0.0, 0.20, 0.24, 0.25, 0.28, 0.30,$ and 1.0 from experimental measurements (denoted by red dots). For comparison, the magnetic susceptibilities of the alloy $\text{Au}_{1-x}\text{Pt}_x$, where x increases from 0.0 to 1.0 are also plotted. The blue solid triangles denote the total magnetic susceptibilities for a realistic alloy sample with the SOC parameters $C_1 = C_2 = 1.0$. The picture of a realistic alloy sample $\text{Au}_{0.25}\text{Pt}_{0.75}$ and the related size parameters are the inset.

to 1.0. One may see that as $C_{1(2)}$ are decreased, the total magnetic susceptibility χ of alloy samples is suppressed to negative values, indicating that the diamagnetism in alloys becomes more and more dominant, which is well consistent with the analysis results shown in Fig. 2. While as the factors $C_{1(2)}$ are enhanced, the zero χ tends to appear in the alloy samples with smaller component ratio x of Pt. Peculiarly, as both C_1 and C_2 are equal to 1, the ultralow magnetic susceptibility χ may appear in the alloy samples $\text{Au}_{1-x}\text{Pt}_x$ with $0.2 < x < 0.3$.

To confirm the above theoretical calculations, we plot the calculated magnetic susceptibilities of the alloy samples with $C_{1(2)} = 1$ and experimental observations of no less than 12 alloy samples with different component ratio x in Fig. 5(b). It clearly demonstrates that the total changing trends of χ versus x from the experimental data are well consistent with our calculated results, which supports further that the samples with the scaling factors $C_{1(2)} = 1$ correspond to real alloy systems. Moreover, the total magnetic susceptibilities of two special samples, i.e., the Au and Pt single crystals, are also in good agreement with our theoretical results. These magnetic behaviors verify the validation of our theoretical calculations on magnetic properties of AuPt alloys. Thus, we believe that the AuPt alloys with ultralow magnetic susceptibilities ($\chi < 10^{-6} \text{ cm}^3/\text{mol}$) may appear around the sample of $\text{Au}_{0.75}\text{Pt}_{0.25}$.

To highlight these inspiring findings, we redraw both theoretical and experimental data in the inset of Fig. 5(b), where the alloy samples from $x = 0.2$ to 0.3 are highlighted. Nevertheless, it should be pointed out that for the sample $\text{Au}_{0.75}\text{Pt}_{0.25}$, the χ value from our theoretical calculations is slightly larger than the corresponding value from our experimental measurement, which may be attributed to the additional hybridizations in alloys. Moreover, the experimental results show that the magnetic susceptibility of AuPt alloys displays abrupt changes at about the concentration ratio $x = 0.25$, with which no less than four alloy samples are fabricated. This interesting magnetic behavior may be a consequence of chemical ordering in the AuPt alloy systems. Although we prepare these homogeneous alloys with the same component ratios through fully mixing two components both by cold rolling and by thermal treatment, we still cannot obtain two identical alloy samples. Thus, a minor changing on the spatial distributions of Au and Pt atoms in the alloy samples with the same ratio x leads to a considerable difference in their ultralow magnetic susceptibilities.

Note that the experimental values of magnetic susceptibilities in Fig. 5(b) are obtained by measuring the magnetic moments M versus the magnetic field H . The representative curves for samples $\text{Au}_{0.80}\text{Pt}_{0.20}$, $\text{Au}_{0.75}\text{Pt}_{0.25}$ and $\text{Au}_{0.70}\text{Pt}_{0.30}$ are shown in Fig. 6. The magnetic susceptibilities are extracted from the slopes of M - H curves after removing the effect of residual magnetism as shown in

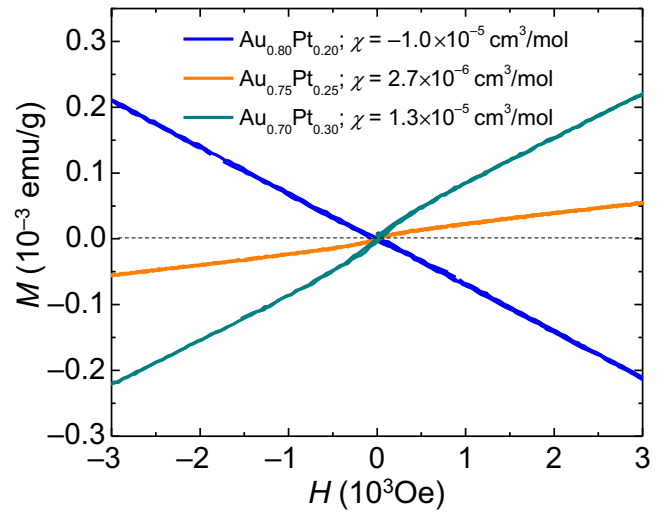


FIG. 6. Experimental measurements on magnetic moments M versus the external magnetic field H in three alloy examples $\text{Au}_{1-x}\text{Pt}_x$ ($x = 0.20, 0.25$, and 0.30).

Fig. S2 within the Supplemental Material [43]. It is clearly shown that curve slope for the $\text{Au}_{0.75}\text{Pt}_{0.25}$ alloy sample is close to zero while the curve slope of the other two samples show opposite values, verifying further that this AuPt alloy sample exhibits an ultralow magnetic susceptibility, which meets the high-standard requirements of the sample applied in precise measurement of gravitation and other special devices.

V. CONCLUSIONS

In summary, we design a series of $\text{Au}_{1-x}\text{Pt}_x$ alloys by using the VCA approach together with the first-principles calculations based on DFT, and calculated their magnetic susceptibility by the *ab initio* calculations within a spin-polarized relativistic SPR CPA. Our theoretical calculations show that the total magnetic susceptibility of AuPt alloys are contributed both by the spin and orbit magnetic susceptibilities of Au and Pt, and the hybridizations between the above two heavy elements play a key role in the different kinds of magnetic susceptibilities in alloys. Moreover, the magnetic structures and the physical origination of spin-, orbit-dependent magnetic susceptibilities, and the SOC-reduced magnetic susceptibilities in Au and Pt are analyzed in detail. Moreover, our theoretical method indicates that the magnetic susceptibility of the AuPt alloy samples can be down to $\chi < 10^{-6} \text{ cm}^3/\text{mol}$, which may occur in the alloy samples around $\text{Au}_{0.75}\text{Pt}_{0.25}$. Following the theoretical expectations, some real AuPt alloy samples possessing the ultralow magnetic susceptibility have been successfully prepared in experiments, and the experimental measurements on the magnetic susceptibilities of some real AuPt alloys are well consistent with our theoretical calculations. The AuPt alloys with ultralow magnetic

susceptibilities constructed here both by our theoretical calculations and experimental fabrications meet well the particular material requirements in TianQin project and other special device applications.

ACKNOWLEDGMENTS

This work is supported by the National Key R&D Program of China (2021YFC2202300), the National Natural Science Foundation of China with Grants No. U20A2077, No. 11774104, and No. 12004003.

-
- [1] O. Jennrich, LISA technology and instrumentation, *Classical Quantum Gravity* **26**, 153001 (2009).
- [2] F. Antonucci, *et al.*, From laboratory experiments to LISA Pathfinder: Achieving LISA geodesic motion, *Classical Quantum Gravity* **28**, 094002 (2011).
- [3] J. Luo, L.-S. Chen, H.-Z. Duan, Y. G. Gong, S. C. Hu, J. H. Ji, Q. Liu, J. W. Mei, V. Milyukov, M. Sazhin, C. G. Shao, V. T. Toth, H. B. Tu, Y. M. Wang, Y. Wang, H. C. Yeh, M. S. Zhan, Y. H. Zhang, V. Zharov, and Z. B. Zhou, TianQin: a SPEAC-borne gravitational wave detector, *Classical Quantum Gravity* **33**, 035010 (2016).
- [4] X. C. Hu, X. H. Li, Y. Wang, W. F. Feng, M. Y. Zhou, Y. M. Hu, S. C. Hu, J. W. Mei, and C. G. Shao, Fundamentals of the orbit and response for TianQin, *Classical Quantum Gravity* **35**, 095008 (2018).
- [5] H. T. Wang, M. Jiang, A. Sesana, E. Barausse, S. J. Huang, Y. F. Yang, W. F. Feng, Y. Wang, Y. M. Hu, J. W. Mei, and J. Luo, Science with the TianQin observatory: Preliminary results on massive black hole binaries, *Phys. Rev. D* **100**, 043003 (2019).
- [6] W. Su, Y. Wang, Z.-B. Zhou, Y.-Z. Bai, Yan. Guo, C. Zhou, T. Lee, M. Wang, M.-Y. Zhou, T. Shi, H. Yin, and B.-T. Zhang, Analyses of residual accelerations for TianQin based on the global MHD simulation, *Classical Quantum Gravity* **37**, 185017 (2020).
- [7] Q. Li, C. Xue, J. P. Liu, J. F. Wu, S. Q. Yang, C. G. Shao, L. D. Quan, W. H. Tan, L. C. Tu, Q. Liu, H. Xu, L. X. Liu, Q. L. Wang, Z. K. Hu, Z. B. Zhou, P. S. Luo, S. C. Wu, V. Milyukov, and J. Luo, Measurements of the gravitational constant using two independent methods, *Nature* **560**, 582 (2018).
- [8] H. Yin, D.-Y. Tan, M. Hu, S. Wang, T.-Z. Bai, S.-C. Wu, and Z.-B. Zhou, Measurements of Magnetic Properties of Kilogram-Level Test Masses for Gravitational-Wave Detection Using a Torsion Pendulum, *Phys. Rev. Appl.* **15**, 014008 (2021).
- [9] H. Ebert, J. Abart, and J. Voitländer, Magnetic susceptibility of $\text{Au}_x\text{Pt}_{1-x}$, *Z. Phys. Chem. Neue Folge* **144**, 223 (1985).
- [10] O. Lopez-Estrada, B. Zuniga-Gutierrez, E. Selenius, S. Malola, and H. Hakkinen, Magnetically induced currents and aromaticity in ligand-stabilized Au and AuPt superatoms, *Nat. Commun.* **12**, 2477 (2021).
- [11] J. F. Schenck, The role of magnetic susceptibility in magnetic resonance imaging: MRI magnetic compatibility of the first and second kinds, *Med. Phys.* **23**, 815 (1996).
- [12] S. Inui, E. Uyama, and K. Hamada, Volume magnetic susceptibility design and hardness of Au–Ta alloys and Au–Nb alloys for MRI-compatible biomedical applications, *Biomed. Phys. Eng. Express* **3**, 015025 (2017).
- [13] T. Kodama, R. Nakai, K. Goto, K. Shima, and H. Iwata, Preparation of an Au-Pt alloy free from artifacts in magnetic resonance imaging, *Magn. Reson. Imaging* **44**, 38 (2017).
- [14] R. Nakai, K. Goto, K. Shima, T. Kodama, and H. Kodama, Dual-phase Au-Pt alloys free from magnetic susceptibility artifacts in magnetic resonance imaging, *Magn. Reson. Imaging* **85**, 19 (2022).
- [15] A. S. Lapp, Z. Y. Duan, N. Marcella, L. Luo, A. Genc, J. Ringnald, A. L. Frenkel, G. Henkelman, and R. M. Crooks, Experimental and theoretical structural investigation of AuPt nanoparticles synthesized using a direct electrochemical method, *J. Am. Chem. Soc.* **140**, 6249 (2018).
- [16] M. Deng, H. Freyer, and H. Ebert, Spin and orbit magnetic susceptibility of the alloy system $\text{Ag}_x\text{Pt}_{1-x}$, *Solid State Commun.* **114**, 363 (2000).
- [17] L. Ballaiche and D. Vanderbilt, Virtual crystal approximation revisited: Application to dielectric and piezoelectric properties of perovskites, *Phys. Rev. B* **61**, 7877 (2000).
- [18] N. J. Ramer and A. M. Rappe, Virtual-crystal approximation that works: Locating a compositional phase boundary in $\text{Pb}(\text{Zr}_{1-x}\text{Ti}_x)\text{O}_3$, *Phys. Rev. B* **62**, R743 (2000).
- [19] B. Winkler, C. Pickard, and V. Milman, Applicability of a quantum mechanical “virtual crystal approximation” to study Al/Si-disorder, *Chem. Phys. Lett.* **362**, 266 (2002).
- [20] G. Geneste, J.-M. Kiat, and C. Malibert, First-principles calculations of quantum paraelectric $\text{La}_{1/2}\text{Na}_{1/2}\text{TiO}_3$ in the virtual-crystal approximation: Structural and dynamical properties, *Phys. Rev. B* **77**, 052106 (2008).
- [21] H. Ebert, A spin polarized relativistic Korringa-Kohn-Rostoker (SPR-KKR) code for Calculating Solid State Properties, version 7.7, D-81377 München, Germany (2017).
- [22] M. Deng, H. Freyer, J. Voitländer, and H. Ebert, Relativistic calculation of magnetic linear response functions using the Korringa-Kohn-Rostoker Green’s function method, *J. Phys.: Condens. Matter* **13**, 8551 (2001).
- [23] H. Ebert, D. Ködderitzsch, and J. Minár, Calculating condensed matter properties the KKR-Green’s function method-recent developments and applications, *Rep. Prog. Phys.* **74**, 096501 (2011).
- [24] J. Staunton, B. L. Gyorffy, and P. Weinberger, On the electronic structure of random metallic alloys containing heavy elements: a relativistic theory, *J. Phys. F: Met. Phys.* **10**, 2665 (1980).
- [25] P. J. Durham, B. L. Gyorffy, and A. J. Pindor, On the fundamental equations of the Korringa-Kohn-Rostoker (KKR) version of the coherent potential approximation (CPA), *J. Phys. F: Met. Phys.* **10**, 661 (1980).
- [26] S. H. Vosko, L. Wilk, and M. Nusair, Accurate spin-dependent electron liquid correlation energies for local spin calculations: A critical analysis, *Can. J. Phys.* **58**, 12003 (1980).
- [27] M. Stener, S. Furlan, and P. Decleva, Density functional calculations of photoionization with an exchange-

- correlation potential with the correct asymptotic behavior, *J. Phys. B: At. Mol. Opt. Phys.* **33**, 1081 (2000).
- [28] W. P. Davey, Precision measurements of the lattice constants of twelve common metals, *Phys. Rev.* **25**, 753 (1925).
- [29] G. De and C. N. R. Rao, Au-Pt alloy nanocrystals incorporated in silica films, *J. Mater. Chem.* **15**, 891 (2005).
- [30] J. Spreadborough and J. W. Christian, High-temperature x-ray diffractometer, *J. Sci. Instrum.* **36**, 116 (1959).
- [31] P. Weinberger, J. Staunton, and B. L. Györfy, A relativistic theory of electronic structure in $\text{Au}_c\text{Pt}_{1-c}$ alloys, *J. Phys. F: Met. Phys.* **12**, 2229 (1982).
- [32] W. H. Butler, Theory of electronic transport in random alloys: Korringa-Kohn-Rostoker coherent-potential approximation, *Phys. Rev. B* **31**, 3260 (1985).
- [33] P. A. Korzhavii, A. V. Ruban, I. A. Abrikosov, and H. L. Skriver, Medelung energy for random metallic alloys in the coherent potential approximation, *Phys. Rev. B* **51**, 5773 (1995).
- [34] I. A. Abrikosov and B. Johansson, Applicability of the coherent-potential approximation in the theory of random alloys, *Phys. Rev. B* **57**, 14164 (1998).
- [35] D. A. Rowlands, J. B. Staunton, and B. L. Györfy, Korringa-Kohn-Rostoker coherent-potential approximation, *Phys. Rev. B* **67**, 115109 (2003).
- [36] S. Mankovsky and H. Ebert, Theoretical description of the high-field susceptibility of magnetically ordered transition metal systems with applications to Fe, Co, Ni, and $\text{Fe}_{1-x}\text{Co}_x$, *Phys. Rev. B* **74**, 054414 (2006).
- [37] S. Polesya, S. Mankovsky, O. Sipr, W. Meindl, C. Strunk, and H. Ebert, Finite-temperature magnetism of $\text{Fe}_x\text{Pd}_{1-x}$ and $\text{Co}_x\text{Pt}_{1-x}$ alloys, *Phys. Rev. B* **82**, 214409 (2010).
- [38] S. N. Khan, J. B. Staunton, and G. M. Stocks, Statistical physics of multicomponent alloys using KKR-CPA, *Phys. Rev. B* **93**, 054206 (2016).
- [39] V. Raghuraman, Y. Wang, and M. Widom, Averaged cluster approach to including chemical short-range order in KKR-CPA, *Phys. Rev. B* **102**, 054207 (2020).
- [40] S. Mankovsky, I. Bakonyi, and H. Ebert, Magnetic susceptibility contributions and electronic density of states in $(\text{Ti}, \text{Zr})_{100-x}(\text{Ni}, \text{Cu})_x$ metallic glasses and crystalline compounds, *Phys. Rev. B* **76**, 184405 (2007).
- [41] H. Ebert, H. Freyer, and M. Deng, Manipulation of the spin-orbit coupling using the Dirac equation for spin-dependent potentials, *Phys. Rev. B* **56**, 9454 (1997).
- [42] H. Ebert, H. Freyer, A. Vernes, and G.-Y. Guo, Manipulation of the spin-orbit coupling using the Dirac equation for spin-dependent potentials, *Phys. Rev. B* **53**, 7721 (1996).
- [43] See Supplemental Material at <http://link.aps.org/supplemental/10.1103/PhysRevApplied.19.034080> for the additional XRD, GDMS, and ICP measurements on Au, Pt, and the AuPt alloy samples.